Available online at www.sciencedirect.com

ScienceDirect

Geochimica et Cosmochimica Acta 125 (2014) 68–84

Geochimica et Cosmochimica Acta

www.elsevier.com/locate/gca

^{224}Ra:^{228}Th disequilibrium in coastal sediments: Implications for solute transfer across the sediment–water interface

Pinghe Cai [a,b,*], Xiangming Shi [a,b], Williard S. Moore [c], Shiyun Peng [a,b], Guizhi Wang [a,b], Minhan Dai [a,b]

[a] State Key Laboratory of Marine Environmental Science, Xiamen University, Xiamen 361005, PR China
[b] College of Ocean and Earth Sciences, Xiamen University, Xiamen 361005, PR China
[c] Department of Earth and Ocean Sciences, University of South Carolina, Columbia, SC 29208, USA

Received 27 March 2013; accepted in revised form 20 September 2013; Available online 2 October 2013

Abstract

We utilized $^{224}Ra/^{228}Th$ disequilibrium in the sediment to investigate processes that regulate solute transfer across the sediment–water interface. Depth profiles of dissolved and surface-bound ^{224}Ra and ^{228}Th in the upper 0–20 cm sediment column were measured using a delayed coincidence counter during a cruise to the Yangtze estuary from 15 to 24 August 2011. Along with ^{224}Ra and ^{228}Th, depth profiles of ^{234}Th were collected to determine the bioturbation rate in the sediment. At most study sites, a significant deficit of ^{224}Ra relative to ^{228}Th was observed in the upper 0–10 cm. In contrast, ^{224}Ra was in excess with respect to ^{228}Th in the upper 0–5 cm at the river mouth, possibly due to redistribution of ^{224}Ra from the mid-salinity region. By modeling the ^{224}Ra depth profiles in the sediment using the general diagenetic equation, we demonstrated that in most cases molecular diffusion and bioturbation together can account for only ~20–30% of the measured flux of ^{224}Ra. We concluded that other mechanisms, especially irrigation, must be invoked to explain the remnant 70% of the observed deviation of ^{224}Ra relative to ^{228}Th. On the basis of the $^{224}Ra/^{228}Th$ disequilibrium in the sediment and a concept of increased surface area for exchange by irrigation as developed by early investigators, we proposed a new approach – the $^{224}Ra/^{228}Th$ disequilibrium approach to quantify the transfer rate of other dissolved species across the sediment–water interface. We have utilized this new approach to determine the benthic consumption rate of dissolved O_2. The result reveals that benthic consumption is an important loss term of dissolved O_2 in the Yangtze estuary and must be considered as one of the mechanisms that lead to hypoxia in this area.

1. INTRODUCTION

The sediment–water interface is a site of intense interaction among physical, biological, and chemical processes. Sediment interstitial waters are typically distinct in chemical composition from the overlying seawater. Consequently, there are generally sharp concentration gradients across the sediment–water interface in many dissolved species. Through diffusion and advection, these dissolved species transfer between the sediment and the overlying water. Early studies have shown that the transfer across the sediment–water interface can have a major effect on the composition of the overlying water. For instance, Sayles (1979) demonstrated that in deep-sea sediments the exchange across the sediment–water interface adds or subtracts Mg^{2+}, K^+, Ca^{2+}, and HCO_3^- from seawater at rates that are of the same order of magnitude as the rates by which these species are added to the oceans by rivers. Thus, it is important to quantify the rates of transfer across the sediment–water interface and to understand the processes that regulate them.

Traditionally, rates of transfer across the sediment–water interface have been determined by (1) deploying a benthic chamber over the sediment to monitor the flux into

* Corresponding author at: State Key Laboratory of Marine Environmental Science, Xiamen University, Xiamen 361005, PR China. Tel.: +86 592 2880179; fax: +86 592 2180655.
E-mail address: Caiph@xmu.edu.cn (P. Cai).

0016-7037/$ - see front matter © 2013 Elsevier Ltd. All rights reserved.
http://dx.doi.org/10.1016/j.gca.2013.09.029

the overlying water (e.g., Berelson et al., 1987; Jahnke et al., 2000), (2) modeling the depth profiles of a dissolved species of interest in the sediment (e.g., Emerson et al., 1984; Lettmann et al., 2012), or (3) constructing a mass balance for a substance in the overlying water column (e.g., Moore and Krest, 2004). Most recently, a thorium series nuclide pair, $^{224}Ra/^{228}Th$, was proposed as a potential approach for tracing the exchange across the sediment–water interface (Cai et al., 2012). In marine sediments, ^{224}Ra (half-life = 3.66 d) is continuously produced via alpha decay by its parent nuclide, ^{228}Th (half-life = 1.91 y). But, unlike the highly particle-reactive ^{228}Th, an appreciable fraction of ^{224}Ra in sediment particles can be released to the interstitial water, and migrate across the sediment–water interface into the overlying water. As a consequence, a deficit of ^{224}Ra with respect to ^{228}Th in near-surface sediments is anticipated. Furthermore, the extent of the ^{224}Ra deficit must be regulated by the multiple processes that operate at the sediment–water interface. As such, investigations on the $^{224}Ra/^{228}Th$ disequilibrium in near-surface sediments will lend insights into both the rate of transfer across the sediment–water interface and the regulating processes therein (e.g., diffusion and bioturbation). Compared to the traditional approaches, the $^{224}Ra/^{228}Th$ disequilibrium method avoids the risk of altering the physical conditions near the sediment–water interface and unlike the modeling approach, makes few assumptions. It is also relatively easy to apply.

Due to prior analytical difficulties, however, there are few measurements on $^{224}Ra/^{228}Th$ disequilibrium in marine sediments. In this study, we utilize a newly developed method (Cai et al., 2012) to investigate the $^{224}Ra/^{228}Th$ disequilibrium in near-surface sediments within the Yangtze River estuary. Our goal is to exploit $^{224}Ra/^{228}Th$ disequilibrium as a proxy for tracing the processes that regulate the transfer of dissolved substances across the sediment–water interface.

2. SAMPLING AND ANALYTICAL METHODS

2.1. Study area

The Yangtze (Changjiang) River is one of the largest rivers in the world with an annual water discharge of 0.9×10^{12} m^3 y^{-1} (Changjiang Sediment Bulletin in 2009, 2010). Historically, the river discharged $\sim 500 \times 10^6$ tons of sediment to the sea annually (Chen et al., 2001). In the last decade, however, the sediment discharge has decreased by 30–40% due to dam and reservoir construction (Yang et al., 2007). Approximately 40% of the total Yangtze-derived sediment is believed to be trapped in the Yangtze estuary (Milliman et al., 1985). Consequently, the Yangtze estuary is characterized by a large fluvial depositional basin. The bottom sediments in the river mouth area (<10 m water depth) are sand and silt, whereas the mid-estuary region (10–60 m water depth) contains a mixture of silt and clay. Further offshore, relic sand of the Pleistocene dominates (Liu et al., 2006). This area is under the influence of strong tidal current, which can be >2 m s^{-1} during spring tide. Coastal oceanography in this area is characterized by a relatively cold and brackish southward-flowing current, the China Coastal Current. This current intensifies in winter, carrying the Yangtze's brackish water and sediment southward along the inner shelf. Over the outer shelf, the sea is dominated by a north flow of warm and saline water, the Taiwan Warm Current, which intensifies in summer in response to the prevailing southeast monsoon (Lee and Chao, 2003).

Crustacea, echinoderms and polychaetes are the main benthic fauna in this region. Seasonal differences in the benthic community have been documented (Liu, 1988). Crustacean and echinoderm were reported to be dominant in summer, and polychaetes were found to dominate the benthic community in winter. The biomass of the benthic fauna is generally high in summer, which can be >40 g/m^2. In comparison, it is much lower in winter (Liu, 1988). Incubation experiments demonstrated that in this region, the benthic fauna can significantly increase the transfer rate of dissolved species, especially ammonia, across the sediment–water interface (Liu, 2007).

2.2. Sample collection

Sediment samples were collected during a cruise to the Yangtze estuary from 15 to 24 August 2011 onboard R/V Runjiang I. Sampling stations are indicated in Fig. 1. Detailed information about the sampling stations is provided in Table 1. A total of 9 stations were occupied during this cruise. Sediment cores were taken from a standard box corer (20 × 20 × 60 cm). The cores were checked visually to ensure that the interface was intact. Each core was sub-sampled for various analyses including ^{224}Ra, ^{228}Th, ^{234}Th, porosity, and grain size. Along the salinity gradient, seawater samples (20 l) were collected and suspended particles were filtered onto a 142-mm 0.7 μm (nominal pore size) GFF filter. The samples were obtained to characterize the disequilibrium between ^{224}Ra and ^{228}Th in suspended particles. In parallel to the sediment coring, depth profiles of ^{224}Ra were collected in the overlying water column. The seawater ^{224}Ra measurements were conducted to investigate the submarine groundwater discharge (SGD) in this

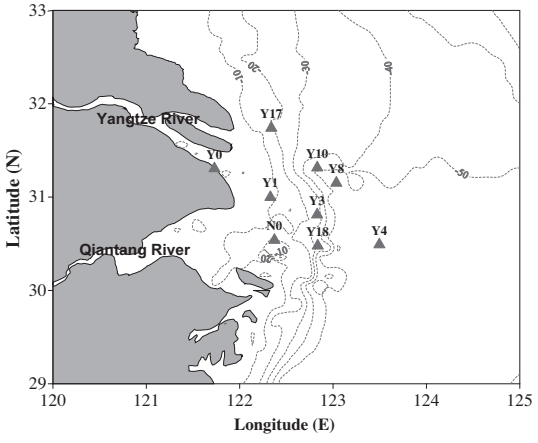

Fig. 1. Location of sampling sites.

Table 1
^{224}Ra, ^{228}Th, and $^{234}Th_{ex}$ activities (dpm/g dry sediment), as well as porosity and grain size in the near-surface sediment of the Yangtze estuary.

Depth (cm)	^{224}Ra (dpm/g)	^{228}Th (dpm/g)	$^{224}Ra/^{228}Th$	$^{234}Th_{excess}$ (dpm/g)	Porosity	Grain size (Ø)
Y0; 31° 19.300′ N, 121° 43.866′ E; 10.0 m; T = 29.21 °C, S = 0.20; August 17, 2011[a]						
0–1	0.79 ± 0.04	0.60 ± 0.03	1.32 ± 0.09	ND	0.377	2.2
2–3	0.86 ± 0.05	0.61 ± 0.03	1.41 ± 0.10	ND	0.407	2.2
4–5	0.81 ± 0.04	0.62 ± 0.03	1.29 ± 0.09	ND	0.418	2.2
6–7	0.74 ± 0.04	0.69 ± 0.03	1.07 ± 0.08	ND	0.438	2.2
10–11	0.68 ± 0.04	0.66 ± 0.03	1.03 ± 0.07	ND	0.462	2.8
15–16	0.66 ± 0.04	0.64 ± 0.03	1.03 ± 0.08	ND	0.443	2.2
Y1; 31° 0.900′ N, 122° 19.685′ E; 12.0 m; T = 25.96 °C, S = 23.06; August 17, 2011						
0–1	0.50 ± 0.05	0.33 ± 0.03	1.52 ± 0.21	ND	0.586	4.2
1–2	0.83 ± 0.07	0.89 ± 0.06	0.93 ± 0.10	ND	0.533	5.3
2–3	0.76 ± 0.07	0.87 ± 0.06	0.87 ± 0.10	ND	0.573	5.1
3–4	0.84 ± 0.07	0.81 ± 0.06	1.04 ± 0.12	ND	0.622	5.2
4–5	0.68 ± 0.06	0.84 ± 0.06	0.82 ± 0.10	ND	0.641	5.7
5–6	0.69 ± 0.06	0.79 ± 0.05	0.88 ± 0.10	ND	0.627	6.4
7–8	0.71 ± 0.07	0.67 ± 0.05	1.05 ± 0.13	ND	0.627	5.3
9–10	0.84 ± 0.09	0.82 ± 0.06	1.03 ± 0.13	ND	0.591	5.9
11–12	0.70 ± 0.09	0.67 ± 0.05	1.05 ± 0.16	ND	0.566	6.0
17–18	0.59 ± 0.08	0.58 ± 0.04	1.03 ± 0.15	ND	0.595	6.2
Y3; 30° 50.337′ N, 122° 49.540′ E; 23.0 m; T = 23.36 °C, S = 30.25; August 19, 2011						
0–0.5	0.66 ± 0.06	1.12 ± 0.08	0.59 ± 0.07	1.64 ± 0.14	0.747	6.3
0.5–1				1.41 ± 0.12	0.733	
1–2	0.70 ± 0.06	1.04 ± 0.07	0.68 ± 0.08	1.12 ± 0.11	0.719	6.3
2–3	1.03 ± 0.09	1.19 ± 0.08	0.87 ± 0.10	0.86 ± 0.10	0.699	6.3
3–4	0.78 ± 0.07	0.93 ± 0.07	0.83 ± 0.09	0.52 ± 0.08	0.658	6.4
4–5	0.49 ± 0.04	0.51 ± 0.04	0.96 ± 0.11	0.00 ± 0.60	0.647	6.0
5–6	0.41 ± 0.03	0.38 ± 0.03	1.09 ± 0.12	ND	0.650	5.9
7–8	0.38 ± 0.04	0.38 ± 0.03	0.99 ± 0.13	ND	0.624	5.8
9–10	0.38 ± 0.04	0.39 ± 0.03	0.98 ± 0.12	ND	0.589	4.4
12–13	0.53 ± 0.05	0.60 ± 0.04	0.88 ± 0.11	ND	0.548	4.9
15–16	0.48 ± 0.05	0.51 ± 0.04	0.93 ± 0.12	ND	0.612	6.4
Y4; 30° 30.477′ N, 123° 20.906′ E; 56.0 m; T = 19.68 °C, S = 34.39; August 20, 2011						
0–0.5	0.56 ± 0.05	0.63 ± 0.05	0.89 ± 0.10	2.54 ± 0.20	0.489	3.0
0.5–1				0.00 ± 0.74	0.446	
1–2	0.36 ± 0.03	0.40 ± 0.03	0.91 ± 0.10	ND	0.444	2.4
2–3	0.36 ± 0.03	0.39 ± 0.03	0.93 ± 0.10	ND	0.442	3.3
3–4	0.28 ± 0.02	0.36 ± 0.03	0.78 ± 0.09	ND	0.449	3.4
4–5	0.32 ± 0.03	0.36 ± 0.03	0.89 ± 0.10	ND	0.427	2.6
5–6	0.31 ± 0.03	0.36 ± 0.03	0.85 ± 0.09	ND	0.420	2.8
7–8	0.38 ± 0.03	0.39 ± 0.03	0.98 ± 0.11	ND	0.412	2.9
9–10	0.43 ± 0.04	0.36 ± 0.03	1.20 ± 0.13	ND	0.408	3.0
11–12	0.42 ± 0.04	0.43 ± 0.03	0.99 ± 0.11	ND	0.403	2.9
14–15	0.35 ± 0.03	0.37 ± 0.03	0.93 ± 0.11	ND	0.382	3.5
Y8; 31° 10.004′ N, 123° 2.221′ E; 63.0 m; T = 20.74 °C, S = 33.70; August 21, 2011						
0–0.5	0.51 ± 0.04	0.60 ± 0.04	0.85 ± 0.09	2.82 ± 0.22	0.518	2.5
0.5–1				2.99 ± 0.23	0.535	
1–2	0.43 ± 0.03	0.49 ± 0.04	0.87 ± 0.09	1.31 ± 0.15	0.512	2.9
2–3	0.37 ± 0.03	0.42 ± 0.03	0.88 ± 0.10	0.07 ± 0.11	0.478	2.8
3–4	0.30 ± 0.03	0.35 ± 0.02	0.87 ± 0.09	0.00 ± 0.25	0.446	3.2
4–5	0.40 ± 0.03	0.43 ± 0.03	0.93 ± 0.10	ND	0.437	2.8
5–6	0.27 ± 0.03	0.34 ± 0.02	0.81 ± 0.09	ND	0.434	2.4
7–8	0.40 ± 0.04	0.43 ± 0.03	0.92 ± 0.11	ND	0.464	2.8
9–10	0.35 ± 0.03	0.33 ± 0.02	1.04 ± 0.12	ND	0.451	2.5
14–15	0.38 ± 0.03	0.43 ± 0.03	0.90 ± 0.10	ND	0.437	3.7
Y10; 31° 19.902′ N, 122° 49.818′ E; 53.0 m; T = 22.70 °C, S = 32.79; August 16, 2011						
0–0.5	0.74 ± 0.06	0.93 ± 0.06	0.79 ± 0.08	5.07 ± 0.35	0.651	4.9
0.5–1				3.55 ± 0.25	0.623	
1–2	0.57 ± 0.04	0.64 ± 0.05	0.90 ± 0.09	0.40 ± 0.10	0.632	5.0
2–3	0.49 ± 0.04	0.53 ± 0.04	0.93 ± 0.10	3.99 ± 0.28 (?)	0.580	4.3

(continued on next page)

Table 1 *continued*

Depth (cm)	^{224}Ra (dpm/g)	^{228}Th (dpm/g)	^{224}Ra/^{228}Th	^{234}Th$_{excess}$ (dpm/g)	Porosity	Grain size (Ø)
3–4	0.38 ± 0.03	0.46 ± 0.03	0.83 ± 0.09	3.05 ± 0.23 (?)	0.574	4.7
4–5	0.47 ± 0.04	0.45 ± 0.04	1.04 ± 0.11	0.01 ± 0.05	0.498	4.0
5–6	0.42 ± 0.03	0.49 ± 0.04	0.86 ± 0.09	ND	0.488	4.8
7–8	0.40 ± 0.03	0.41 ± 0.03	0.97 ± 0.11	ND	0.471	5.0
9–10	0.34 ± 0.03	0.37 ± 0.03	0.91 ± 0.10	ND	0.471	5.3
11–12	0.43 ± 0.04	0.49 ± 0.03	0.87 ± 0.09	ND	0.421	4.6
Y17; 31° 45.359′ N, 122° 20.561′ E; 23.0 m; T = 23.10 °C, S = 30.49; August 16, 2011						
0–0.5	0.90 ± 0.07	1.01 ± 0.07	0.89 ± 0.09	1.54 ± 0.14	0.642	6.4
0.5–1				1.13 ± 0.12	0.652	
1–2	1.00 ± 0.13	0.87 ± 0.07	1.14 ± 0.18	1.35 ± 0.13	0.646	5.0
2–3	0.71 ± 0.11	0.77 ± 0.06	0.92 ± 0.16	0.93 ± 0.11	0.581	5.0
3–4	0.56 ± 0.05	0.85 ± 0.06	0.65 ± 0.07	0.20 ± 0.09	0.539	5.1
4–5	0.34 ± 0.03	0.53 ± 0.04	0.63 ± 0.07	0.40 ± 0.06	0.544	5.1
5–6	0.54 ± 0.04	0.61 ± 0.04	0.89 ± 0.09	0.00 ± 0.20	0.557	6.0
7–8	0.61 ± 0.05	0.65 ± 0.05	0.94 ± 0.10	ND	0.526	5.6
9–10	0.63 ± 0.05	0.69 ± 0.05	0.92 ± 0.10	ND	0.596	5.9
11–12	0.72 ± 0.06	0.72 ± 0.05	1.01 ± 0.11	ND	0.587	6.6
14–15	0.69 ± 0.06	0.69 ± 0.05	1.01 ± 0.11	ND	0.596	6.6
17–18	0.64 ± 0.05	0.69 ± 0.05	0.93 ± 0.10	ND	0.553	5.6
Y18; 30° 30.330′ N, 122° 49.779′ E; 23.0 m; T = 20.48 °C, S = 33.82; August 22, 2011						
0–0.5	0.87 ± 0.07	0.89 ± 0.06	0.98 ± 0.11	5.16 ± 0.34	0.767	6.0
0.5–1				2.53 ± 0.19	0.739	5.9
1–2	0.76 ± 0.06	0.88 ± 0.06	0.86 ± 0.09	0.80 ± 0.10	0.730	6.0
2–3	0.71 ± 0.06	0.74 ± 0.05	0.96 ± 0.10	0.53 ± 0.08	0.706	6.2
3–4	0.45 ± 0.04	0.52 ± 0.04	0.86 ± 0.10	0.31 ± 0.08	0.686	6.4
4–5	0.64 ± 0.05	0.63 ± 0.05	1.02 ± 0.11	0.18 ± 0.06	0.650	6.1
5–6	0.38 ± 0.03	0.47 ± 0.03	0.81 ± 0.09	0.21 ± 0.06	0.607	6.0
7–8	0.58 ± 0.05	0.52 ± 0.04	1.10 ± 0.12	ND	0.603	5.9
9–10	0.39 ± 0.03	0.36 ± 0.03	1.11 ± 0.13	ND	0.651	4.6
11–12	0.48 ± 0.04	0.45 ± 0.04	1.06 ± 0.12	ND	0.634	6.0
14–15	0.33 ± 0.03	0.36 ± 0.03	0.93 ± 0.11	ND	0.592	5.8
N0; 30° 30.368′ N, 122° 22.341′ E; 26.0 m; T = 25.51 °C, S = 26.78; August 18, 2011						
0–0.5	0.52 ± 0.04	0.49 ± 0.04	1.07 ± 0.11	ND	0.631	5.9
0.5–1				ND	0.615	
1–2	0.52 ± 0.04	0.49 ± 0.04	1.06 ± 0.11	ND	0.568	5.8
2–3	0.53 ± 0.04	0.48 ± 0.03	1.09 ± 0.12	ND	0.589	5.7
3–4	0.45 ± 0.04	0.37 ± 0.03	1.20 ± 0.13	ND	0.574	5.6
4–5	0.40 ± 0.04	0.38 ± 0.03	1.06 ± 0.12	ND	0.582	5.9
5–6	0.41 ± 0.04	0.39 ± 0.03	1.04 ± 0.12	ND	0.578	6.1
7–8	0.47 ± 0.04	0.42 ± 0.03	1.14 ± 0.13	ND	0.562	5.5
9–10	0.40 ± 0.03	0.37 ± 0.03	1.10 ± 0.12	ND	0.564	5.1
11–12	0.53 ± 0.05	0.55 ± 0.04	0.98 ± 0.11	ND	0.494	4.9
14–15	0.47 ± 0.04	0.48 ± 0.04	0.98 ± 0.11	ND	0.500	4.5

ND: Not detectable, i.e., when the second measurement of sediment ^{234}Th is larger or indistinguishable from the first measurement.
[a] *T* and *S* represent temperature and salinity in the bottom water.

area. The results will be reported elsewhere (Wang et al., personal communication).

2.3. ^{224}Ra and ^{228}Th analyses

The method for the determination of ^{224}Ra and ^{228}Th in coastal sediments has been described in detail by Cai et al. (2012). This technique measures ^{224}Ra and ^{228}Th dissolved in pore water as well as surface-bound ^{224}Ra and ^{228}Th. It does not detect ^{224}Ra and ^{228}Th bound in the crystal lattice of bulk sediments. In brief, immediately after sample collection, the sediment sub-cores (area = 17.3 cm^2) were sliced into 1-cm thick slabs. The sediment slab was placed in a 250 ml Teflon beaker and 150 ml Milli-Q water was added to form a slurry. The slurry was ultrasonicated for 5 min. To the slurry 5–10 drops of concentrated $NH_3{\cdot}H_2O$ were added. Then, 1.0 ml of $KMnO_4$ solution (3.0 g l^{-1}) and 1.0 ml of $MnCl_2$ solution (8.0 g $MnCl_2{\cdot}4H_2O$ l^{-1}) were added to form a suspension of MnO_2. Subsequently, the sediment slurry together with the MnO_2 precipitate was filtered onto a pre-weighed 142-mm 0.7 μm (nominal pore size) GFF filter. The filtration was terminated when droplets of water ceased to issue from the filter. The sample was then placed into the sample chamber and was partially

dried for ~30 min using an air stream. After the weight ratio of water/(sediment + filter) was adjusted to 0.4–0.5, we recorded the weight of the sample and connected the sample chamber to the RaDeCC system. Helium gas was circulated through the sediment sample and the counting cell at a rate of 12–15 l/min. The sample was counted for 4–6 h. About 8–10 d later, the sample was re-measured using a same RaDeCC system. In order to minimize the error, the water content of the sample was maintained in the vicinity of the original level during storage. The measurement parameters (like water content, counting time, etc.) were also controlled to be consistent in the two measurements. The final ^{224}Ra and ^{228}Th activities at the sampling time were calculated from the first and the second measurements. Chance coincidence and contributions from the 219 channel were corrected using the equations described in Moore and Arnold (1996) and Moore (2008). The errors associated with ^{224}Ra and ^{228}Th activities were propagated from counting statistics, counter calibration, chance coincidence correction and in-growth correction. The RaDeCC counter is calibrated with a ^{232}U–^{228}Th standard using the method of standard addition. The reproducibility and the overall accuracy of ^{224}Ra (and ^{228}Th) measurement based on this method are estimated to be ±5% and ±5–7%, respectively. Finally, it must be noted that the ^{224}Ra and ^{228}Th measurements actually represent the exchangeable ^{224}Ra activity and the production rate of exchangeable ^{224}Ra in sediment particles. For convenience, however, hereafter we simply refer to them as ^{224}Ra and ^{228}Th activities.

2.4. $^{234}Th_{ex}$ analysis

Excess ^{234}Th ($^{234}Th_{ex}$) activity in the sediment was acquired from two parallel measurements. Immediately after the cruise, dried sediment samples (3–4 g) were leached in a hot solution of 50 ml of 6 N HCl + 5 ml of H_2O_2 for 4 h. To ensure that the absorbed ^{234}Th was quantitatively leached, this step was repeated 3 times. Subsequently, the leachates were combined and evaporated to near dryness. Twenty milliliters of 8 N HNO_3 was added to re-dissolve the sample, which was then transferred into a preconditioned anion-exchange column (AG1-X8, 100–200 mesh). Thorium was purified by rinsing the column with 3 × 10 ml of 8 N HNO_3 (Anderson and Fleer, 1982). Final ion-exchange chemistry was accomplished by passing 3 × 10 ml of 1 N HCl to elute the Th into a 100 ml beaker. Then, $NH_3{\cdot}H_2O$ was added to the Th effluent and the pH was adjusted to ~9.0. The subsequent procedure is essentially similar to the protocol for seawater ^{234}Th measurement based on the MnO_2 co-precipitation technique (e.g., Buesseler et al., 2001; Cai et al., 2006). Briefly, 0.375 ml of $KMnO_4$ solution (3.0 g l^{-1}) and 0.25 ml of $MnCl_2$ solution (8.0 g $MnCl_2{\cdot}4H_2O$ l^{-1}) were added to form a suspension of MnO_2, which serves to absorb Th isotopes in the solution. The MnO_2 suspension was filtered onto a 25 mm diameter, 1.0 μm pore size QMA filter. The filter was dried, and mounted under one layer of Mylar film and two layers of aluminum foil. The ^{234}Th activity in the sample was determined immediately by counting its daughter ^{234m}Pa on a gas-flow proportional low-level beta counter (GM-25-5, RISØ National Laboratory, Denmark).

After 5–6 months, a parallel sediment sample was processed in the same manner as described above and the sample was measured using the same RISØ detector. The signal in this parallel measurement is contributed from the ^{234}Th activity that was supported by ^{238}U, non-^{234}Th beta emitters (like ^{212}Pb, ^{212}Bi, ^{208}Tl, and other short-lived beta-emitting daughters of ^{228}Th), and the background of the counter. $^{234}Th_{ex}$ activity was calculated from the two parallel measurements and reported with a propagated uncertainty that includes the two parallel counting of ^{234}Th and the error associated with detector calibration. The detectors were calibrated using deep waters and/or aged seawater samples where ^{234}Th and ^{238}U are expected to be in secular equilibrium (e.g., Rutgers van der Loeff et al., 2011).

Unlike the procedure used by early investigators (e.g., Aller and Cochran, 1976; DeMaster et al., 1985), our protocol for sediment ^{234}Th analysis does not involve a yield tracer. As such, it is important to evaluate the overall yields of the chemical procedure that we applied. The overall yields are determined using the method of standard addition, i.e., by measuring a set of standards in which known activities of ^{234}Th and ^{238}U were added to an unknown sediment sample. Dried sediment samples collected from the Yangtze estuary were mixed and homogenized. A set of 8 replicate samples each with a dried mass of 3.8 g were taken from the homogenized bulk sediment. To the replicate samples a succession (0.500, 1.000, 1.500, 2.000, 2.500, 3.000, 3.500, and 4.000 ml) of ^{238}U–^{234}Th standard solutions with a ^{234}Th activity of 68.5 ± 0.70 dpm/ml were added. The samples were processed and measured following the procedure described above. The results of ^{234}Th measurement vs. ^{234}Th addition from the standards are shown in Fig. 2. A simple Linear Least Square (LLS) analysis is performed. The SLOPE gives an overall yield of 0.963 ± 0.059. The high yield with a relatively small error indicates that our chemical procedure for the $^{234}Th_{ex}$ measurement in sediment is reliable. The standard error associated with the overall yield was also included when propagating the error related to the $^{234}Th_{ex}$ activity. Overall, the reproducibility of the $^{234}Th_{ex}$ measurement based on our procedure is considered to be in the vicinity of ±10%.

2.5. Sedimentology

The box cores were sampled at various depths for grain size analysis, which was performed with a laser particle size analyzer (Melvern's Matersizer 2000). Separate sediment samples were dried at 60 °C for 24 h. The porosity was calculated from the weight loss using a grain density of 2.6 g cm^{-3}.

3. RESULTS

^{224}Ra, ^{228}Th, and $^{234}Th_{ex}$ activities as well as porosity and grain size in the near-surface sediment of the Yangtze estuary are presented in Table 1. Bottom water temperature and salinity at each station are also presented. During the cruise, bottom water temperature at the study sites varied

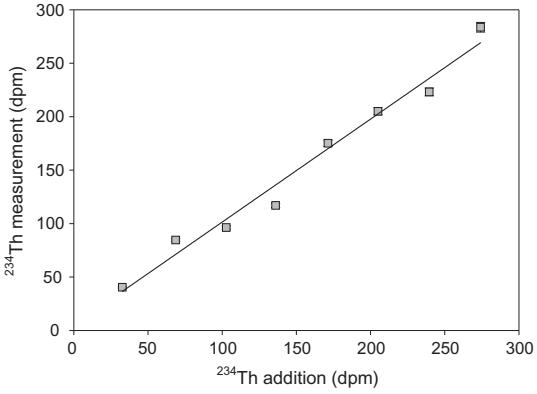

Fig. 2. The overall yields of the chemical procedure for ^{234}Th in the sediment determined using the method of standard addition. Note that error bars are generally smaller than the symbol size.

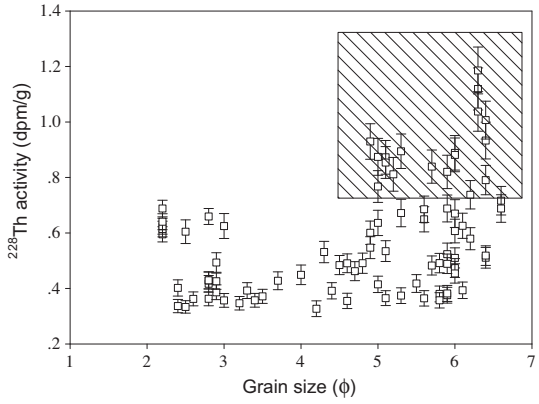

Fig. 3. A plot of ^{228}Th activity vs. grain size in the sediment of the study region. High ^{228}Th data are highlighted in the shadowed box.

between 29.21 and 19.68 °C, and showed a decrease with distance offshore. Bottom water salinity increased with distance offshore, from 0.20 at Y0 to 34.39 at Y4. Porosity in the near-surface sediment ranged from 0.377 to 0.767. Due to sediment compaction, porosity profiles showed a general decrease with depth. Grain size distribution at the study sites ranged from sand to silt, with the coarsest sediment at the river mouth site (Y0). In general, coarse sediments were characterized by lower porosity.

3.1. Depth profiles of ^{224}Ra and ^{228}Th

Sediment ^{228}Th activities at the study sites varied between 0.33 ± 0.03 and 1.19 ± 0.08 dpm/g (dried mass). High ^{228}Th activity was generally found to be associated with fine sediment (Fig. 3). This observation is consistent with the recognition that thorium is principally absorbed onto particle surface and consequently, small particles tend to have a higher absorption capacity for thorium due to their large specific surface area (e.g., Santschi et al., 2006). Except at Y0, Y1, and N0, depth profiles of ^{228}Th show a rapid decrease in the upper 5 cm (Fig. 4). The reduction in ^{228}Th activity is coincident with the depth trend of sediment ^{234}Th$_{ex}$ activity (Table 1), and indicates that a considerable fraction of ^{228}Th in the surface sediment must be supplied via the scavenging of ^{228}Th in the overlying water column by suspended particles. Indeed, Broecker et al. (1973) observed that ^{228}Th/^{228}Ra ratio in surface water was much less than unity and decreased as the coast was approached. Subsequent to deposition of suspended particles at the sediment–water interface, ^{228}Th in excess over that supported by ^{228}Ra in the sediment starts to decay, resulting in a decline of ^{228}Th activity with depth in the near-surface sediment. At Y0 and N0, ^{228}Th activity was relatively constant with depth. At Y1, a ^{228}Th minimum was observed at the sediment surface, but increased a factor of 3 in the underlying sample. Below this layer, ^{228}Th activity slightly decreased with depth. The absence of a decline of ^{228}Th activity with depth suggests that an excess of ^{228}Th relative to ^{228}Ra may not exist at Y0, Y1, and N0. Indeed, at these sites no excess ^{234}Th activity was detectable (Table 1). The absence of sediment ^{228}Th$_{ex}$ and ^{234}Th$_{ex}$ at Y0, Y1, and N0 may be caused by lateral transport of bottom sediment across the estuary. In fact, this process has been demonstrated to be responsible for the formation of a ~800 km subaqueous deltaic deposit that extends from the Yangtze River mouth south toward the Taiwan Strait (Liu et al., 2006). A similar mechanism was invoked to interpret the seabed deficiency in ^{234}Th observed on the Amazon shelf (Moore et al., 1996; Smoak et al., 1996).

Sediment ^{224}Ra activities in the study region ranged from 0.27 ± 0.02 to 1.03 ± 0.09 dpm/g. ^{224}Ra profiles generally show a depth pattern similar to ^{228}Th (Fig. 4). At depths below 10 cm, ^{224}Ra approached secular equilibrium with ^{228}Th. For depths between 10 and 20 cm, the mean ^{224}Ra/^{228}Th activity ratio was 0.993 ± 0.078 (1 SD, $n = 26$), not significantly different from unity. The standard deviation is also consistent with the error propagated from the measurement uncertainty of ^{224}Ra and ^{228}Th (±5%). This indicates that ^{224}Ra migration was negligible below 10 cm. In contrast, a significant deviation of ^{224}Ra relative to ^{228}Th was evident in the upper 0–10 cm at most study sites. The most remarkable deficit of ^{224}Ra occurred at Y3, where at 0–1 cm ^{224}Ra/^{228}Th ratio was as low as 0.59 ± 0.07. The marked deficit in ^{224}Ra indicates active migration of ^{224}Ra across the sediment–water interface into the overlying water column. At Y0, however, ^{224}Ra was in excess with respect to ^{228}Th in the upper 5 cm. Below this layer, ^{224}Ra and ^{228}Th approached secular equilibrium.

3.2. ^{224}Ra and ^{228}Th activities in suspended particles

^{224}Ra and ^{228}Th activities in suspended particles along the salinity gradient in the Yangtze estuary are presented in Table 2. Also presented in Table 2 is ^{224}Ra activity in seawater. Seawater ^{224}Ra activity varied between 5.85 ± 0.12 and 111.2 ± 0.8 dpm/100 l, and exhibited a plateau in the salinity range of 5–15 (Fig. 5). This mode is similar to the pattern of seawater ^{224}Ra vs. salinity in most estuaries (e.g., Krest et al., 1999; Moore and Krest, 2004; Liu et al., 2012). It reflects release of ^{224}Ra into seawater from suspended particles and/or bottom sediment or submarine groundwater discharge. ^{228}Th activity in suspended particles ranged from 1.06 ± 0.16 to 2.24 ± 0.21 dpm/g,

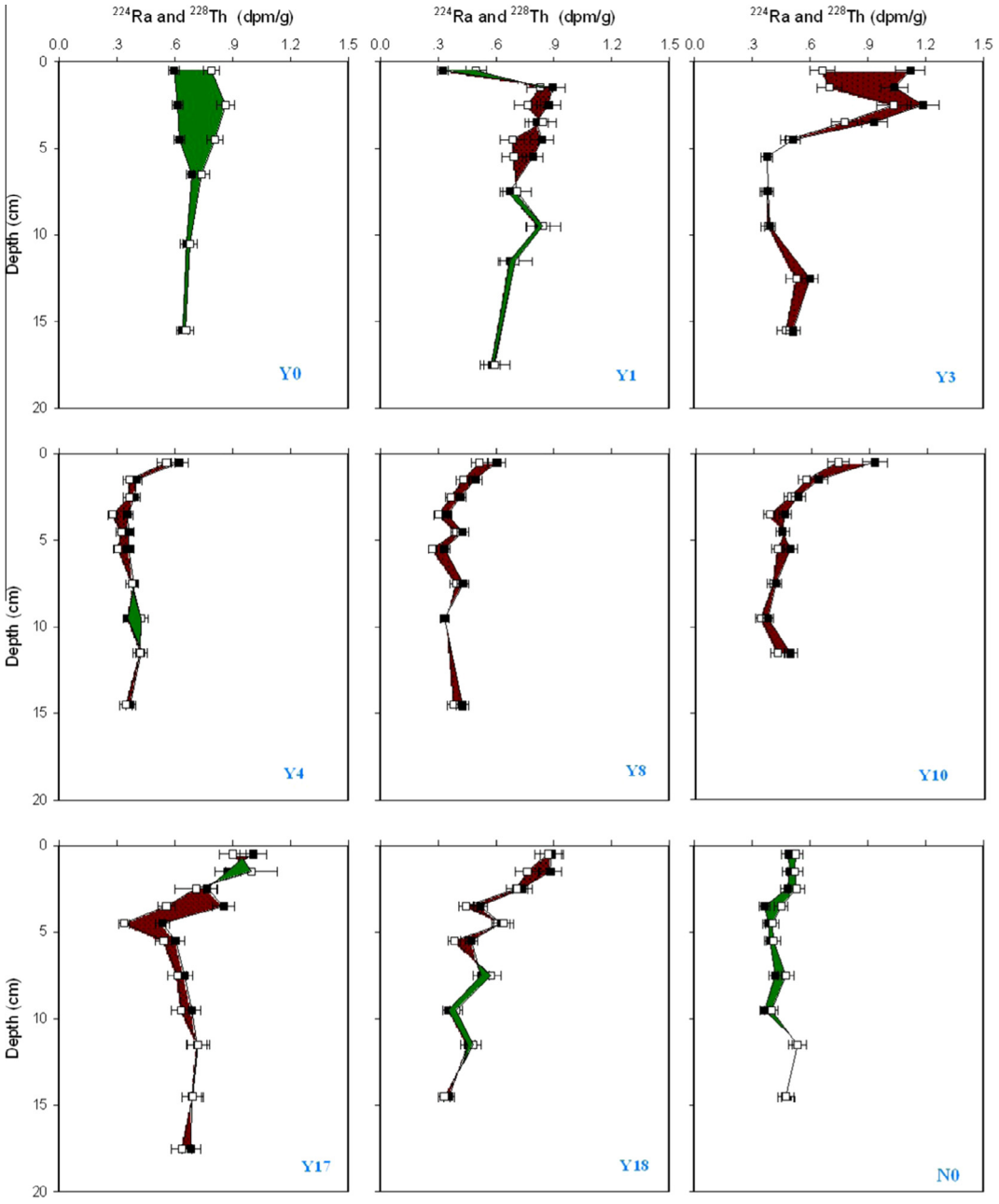

Fig. 4. Depth profiles of ^{224}Ra (open square) and ^{228}Th (filled square) in the upper 0–20 cm sediment. The red area represents a deficit of ^{224}Ra and the green area denotes an excess of ^{224}Ra. (For interpretation of the references to color in this figure legend, the reader is referred to the web version of this article.)

much higher than that in the surface sediment. The difference between suspended and seabed ^{228}Th activity can be due to a grain size effect, with finer-grained suspended matter in water column. It may also reflect that a considerable fraction of ^{228}Th in suspended particles has decayed away or mixed with older sediment after deposition over the seafloor. ^{224}Ra activity in suspended particles varied between 0.48 ± 0.13 and 2.13 ± 0.31 dpm/g. At $S < 2$, ^{224}Ra and ^{228}Th in suspended particles were essentially in secular equilibrium. In comparison, a marked deficit of ^{224}Ra relative to ^{228}Th in suspended particles was observed at $S > 2$ (Fig. 5). The most remarkable depletion of ^{224}Ra in suspended particles occurred at $S = 15.8$, where the ^{224}Ra/^{228}Th ratio was as low as 0.35 ± 0.07. On average, at $S > 2$ the ^{224}Ra/^{228}Th ratio in suspended particles was 0.60 ± 0.21 (1 SD, $n = 5$). This indicates that ~40% of the exchangeable ^{224}Ra in suspended particles desorbed during mixing into seawater. This result compares well with the estimate from a desorption experiment on Yangtze sediment by Gu et al. (2012). It is also consistent with the result from the Amazon shelf, where Moore et al. (1995) showed that 40% of the exchangeable ^{224}Ra in suspended particles was released into

Table 2
^{224}Ra and ^{228}Th activities (dpm/g dry mass) in suspended particles, seawater ^{224}Ra activity, and the K_d value of ^{224}Ra along the salinity gradient in the Yangtze estuary. Samples were collected on August 17, 2011.

Latitude (°N)	Longitude (°E)	Salinity	TSM (mg/L)	Seawater ^{224}Ra (dpm/100 l)	^{224}Ra (dpm/g)	^{228}Th (dpm/g)	^{224}Ra/^{228}Th (A.R.)	K_d[a] (10^4 cm^3/g)
31° 19.300′	121° 43.866′	0.16	170	19.5 ± 0.3	2.13 ± 0.31	2.24 ± 0.21	0.95 ± 0.17	1.06 ± 0.16
31° 06.600′	121° 56.110′	1.70	2050	69.8 ± 0.4	1.73 ± 0.20	1.75 ± 0.13	0.99 ± 0.14	0.25 ± 0.03
31° 04.800′	122° 01.440′	5.60	2207	111.2 ± 0.8	1.22 ± 0.12	1.71 ± 0.12	0.72 ± 0.09	0.11 ± 0.01
31° 03.300′	122° 05.160′	10.3	459	106.7 ± 0.9	1.05 ± 0.13	1.79 ± 0.14	0.59 ± 0.08	0.10 ± 0.01
31° 02.820′	122° 07.200′	15.8	591	107.1 ± 0.8	0.62 ± 0.10	1.77 ± 0.14	0.35 ± 0.07	0.06 ± 0.01
31° 01.500′	122° 15.780′	20.0	269	69.5 ± 0.5	1.48 ± 0.14	1.66 ± 0.16	0.89 ± 0.12	0.21 ± 0.02
31° 00.900′	122° 19.680′	29.0	13.1	5.85 ± 0.12	0.48 ± 0.13	1.06 ± 0.16	0.46 ± 0.14	0.82 ± 0.22

[a] K_d is defined as the ratio of ^{224}Ra activity in suspended particles (dpm/g) to the activity in seawater (dpm/cm^3).

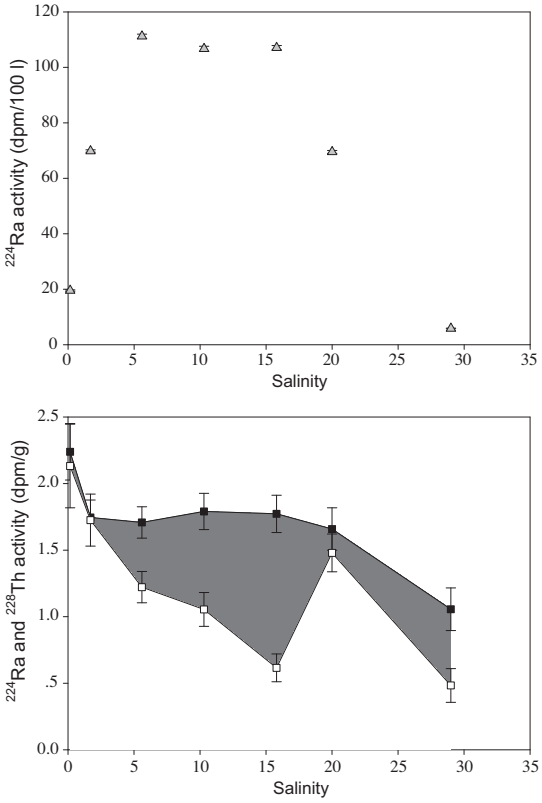

Fig. 5. Distributions of seawater ^{224}Ra activity (upper panel), and ^{224}Ra (open square) and ^{228}Th (closed square) activities in suspended particles (lower panel) along the salinity gradient in the Yangtze estuary.

seawater. Direct measurement of ^{224}Ra and ^{228}Th in suspended particles thus provides an independent approach for quantifying desorption rate of radium during estuarine mixing.

3.3. Depth profiles of ^{234}Th$_{ex}$

Excess ^{234}Th activities (^{234}Th$_{ex}$) were observed in the upper 0–6 cm sediment column at most study sites except for Y0, Y1, and N0 (Table 1). The absence of ^{234}Th$_{ex}$ at these sites, as mentioned above, could be caused by lateral transport of bottom sediment across the estuary. The ^{234}Th$_{ex}$ profiles generally showed a decrease with depth (Fig. 6), which must be ascribed to the decay of ^{234}Th after deposition over the seafloor. There were considerable site-to-site variations in ^{234}Th$_{ex}$. ^{234}Th$_{ex}$ activity in the surface 0–0.5 cm ranged from a low of 1.54 ± 0.14 dpm/g to a high of 5.16 ± 0.34 dpm/g. The inventory of ^{234}Th$_{ex}$ activity in the upper 0–6 cm varied between 1.69 ± 0.15 and 5.33 ± 0.47 dpm/cm^2 (Table 3). At Y10, high ^{234}Th$_{ex}$ activities at depth between 2 and 3 cm were observed below a layer of sediment with low ^{234}Th$_{ex}$ activity. These high ^{234}Th$_{ex}$ activities, however, were not consistent with the depth pattern of ^{228}Th at the same station. We thus consider that the high ^{234}Th$_{ex}$ signal between 2 and 3 cm at Y10 could be a sampling artifact. As such, these abnormal data were not included in the calculation of ^{234}Th inventory.

4. DISCUSSION

4.1. Bioturbation rates estimated from ^{234}Th

Bioturbation is an important process that influences the transfer of dissolved species across the sediment–water interface. In this study, we use a less restrictive definition of bioturbation (Smethie et al., 1981). It refers to any displacement of particles and the accompanying movement of interstitial water, whether initiated by biological or physical processes. In the absence of bioturbation, ^{234}Th$_{ex}$ would be confined in the surface sediment as its half-life (24.1 d) is short compared to the typical sedimentation rate in the coastal areas (~1 cm y^{-1}). The occurrence of ^{234}Th$_{ex}$ at depth in the sediment thus reflects the downward mixing of sediment. Since the 1970s, the penetration of ^{234}Th$_{ex}$ into sediment has been extensively utilized to assess bioturbation rates (e.g., Aller and Cochran, 1976). Assuming steady state and constant porosity, the rate of change in ^{234}Th$_{ex}$ activity is described by the equation

$$\frac{\partial^{234}\mathrm{Th}_{ex}}{\partial t} = 0 = \frac{\partial\left(D_B \frac{\partial^{234}\mathrm{Th}_{ex}}{\partial z}\right)}{\partial z} - \omega\frac{\partial^{234}\mathrm{Th}_{ex}}{\partial z} - \lambda_{234}{}^{234}\mathrm{Th}_{ex} \quad (1)$$

where D_B is the bioturbation coefficient, ω denotes the sedimentation rate, and z represents depth below the sediment–water interface. If the advective burial of sediment is a negligible term for ^{234}Th$_{ex}$ distribution (i.e., $\omega \approx 0$), and if D_B is constant with depth, then we can solve Eq. (1) by taking the

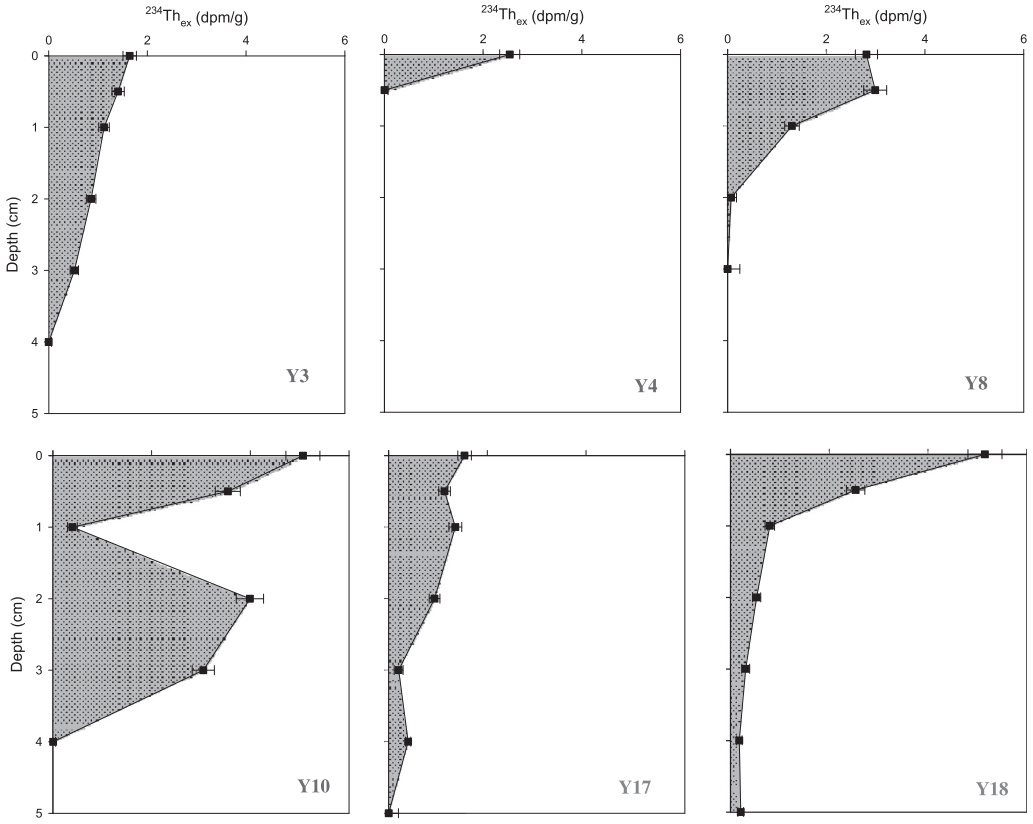

Fig. 6. Depth profiles of $^{234}Th_{ex}$ in the sediment. Note the outliers at 2 and 3 cm at Y10. The two values are excluded when finding the best fit of the $^{234}Th_{ex}$ profile at this station.

Table 3
$^{234}Th_{ex}$ inventory (I $^{234}Th_{ex}$), bioturbation coefficient (D_B), observed flux of ^{224}Ra (F_{Ra}), theoretical flux of ^{224}Ra induced by molecular diffusion (F_M), by molecular diffusion plus bioturbation (F_{M+B}), residence time of pore water (τ), benthic consumption rate of O_2 (F_{O_2}), and utilization rate of O_2 in the bottom of the water column (R_{O_2}) at the study sites.

Station	I $^{234}Th_{ex}$ (dpm cm^{-2})	D_B (10^{-7}cm^2 s^{-1})	F_{Ra} (dpm cm^{-2} d^{-1})	F_M (dpm cm^{-2} d^{-1})	F_{M+B} (dpm cm^{-2} d^{-1})	τ (d)	F_{O_2} (mmol m^{-2} d^{-1})	R_{O_2} (mmol m^{-2} d^{-1})
Y0	–	–	0.419 ± 0.055	0.001	–	0.010 ± 0.001	–	–
Y1	–	–	-0.017 ± 0.046	−0.018	–	–	1.2 ± 3.4	20.6
Y3	2.99 ± 0.16	17	-0.177 ± 0.030	−0.025	−0.053	2.4 ± 0.6	25.6 ± 4.4	40.0
Y4	1.69 ± 0.15	0.002[a]	-0.084 ± 0.034	−0.009	−0.009	1.8 ± 0.8	–	–
Y8	5.33 ± 0.47	4.6	-0.122 ± 0.032	−0.011	−0.023	1.5 ± 0.5	–	–
Y10	4.41 ± 0.22	1.6	-0.121 ± 0.033	−0.016	−0.021	2.1 ± 0.7	21.6 ± 5.8	110.3
Y17	4.20 ± 0.32	20	-0.178 ± 0.046	−0.020	−0.057	2.6 ± 1.0	24.2 ± 6.2	69.6
Y18	4.01 ± 0.18	1.4	-0.031 ± 0.029	−0.018	−0.022	34 ± 105	6.9 ± 6.3	42.8
N0	–	–	0.082 ± 0.028	−0.010	–	–	–	–

[a] At Y4, D_B was estimated by fitting only two data points. This gives an upper limit of D_B at this location.

boundary conditions $^{234}Th_{ex} = [^{234}Th_{ex}]_0$ at $z = 0$ and $^{234}Th_{ex} = 0$ at $z \to \infty$:

$$^{234}Th_{ex} = [^{234}Th_{ex}]_0 e^{-\sqrt{\frac{\lambda_{234}}{D_B}}z} \quad (2)$$

Fitting Eq. (2) to the $^{234}Th_{ex}$ profiles yields the best estimates of D_B. As shown in Table 3, the bioturbation coefficient varied over three orders of magnitude, from $<0.01 \times 10^{-7}$ to 20×10^{-7} cm^2 s^{-1}. The wide range of the D_B values in Table 3 suggests that benthic biological activity was highly heterogeneous in the Yangtze estuary. Overall, the D_B values in this study are comparable to the estimates of the bioturbation coefficient in the New York Bight and the Amazon shelf (e.g., Cochran and Aller, 1979; DeMaster et al., 1980). High values of $D_B (\sim 2 \times 10^{-6}$ cm^2 s$^{-1})$ were observed at Y3 and Y17. These values are similar in magnitude to the molecular diffusion coefficient in sediment interstitial water ($\sim$1–10×10^{-6} cm^2 s^{-1}). This implies that bioturbation could be an important process in regulating the transfer of dissolved species across the sediment–water interface in the Yangtze estuary.

4.2. ^{224}Ra flux across the sediment–water interface

^{224}Ra fluxes across the sediment–water interface at our study sites can be calculated with a one-dimensional (1D) mass balance exchange model (Cai et al., 2012). By assuming steady state and that ^{224}Ra is solely supplied via alpha-decay of ^{228}Th in the sediment, the flux of ^{224}Ra can be directly derived from a mass balance consideration:

$$F_{\mathrm{Ra}} = -\int_0^{\infty} \lambda_{224}(A_{\mathrm{Th}} - A_{\mathrm{Ra}})dz \quad (3)$$

where F_{Ra} (dpm cm^{-2} d^{-1}) denotes the flux of ^{224}Ra ("+" downward) across the sediment–water interface. A_{Th} and A_{Ra} are ^{228}Th and ^{224}Ra activities in a unit of dpm cm^{-3} (wet sediment), which was converted from a mass unit using a relationship of dpm cm^{-3} = dpm g^{-1} × ρ_s × (1 − ø), where ρ_s is the sediment density and ø is the porosity. In practice, we assume that ^{224}Ra and ^{228}Th are in secular equilibrium below 10 cm. $F_{\mathrm{Ra}}$was then calculated by trapezoidal integration of the ^{224}Ra deficit in the bioturbation zone (0–10 cm). As shown in Table 3, ^{224}Ra fluxes varied between -0.178 ± 0.046 and 0.419 ± 0.055 dpm cm^{-2} d^{-1} in our study region.

The positive values, which may result from a net scavenging of ^{224}Ra from the overlying seawater by the bottom sediment, are a reflection of the distinct geochemical behavior of ^{224}Ra in freshwater as compared to seawater. In freshwater the distribution coefficient (K_d) is high, causing ^{224}Ra to be bound tightly onto particle surfaces (e.g., Swarzenski et al., 2003). As river water mixes with seawater, the increasing ionic strength causes K_d to decrease, releasing a considerable fraction of Ra from particles. Thus, the mid-estuary region is generally characterized by elevated activities of dissolved ^{224}Ra. In the Yangtze estuary, seawater ^{224}Ra activity in the mid-salinity region was on the order of 100 dpm/100 l, compared to ~ 20 dpm/100 l at the river mouth (Fig. 5). In contrast, as estimated from the ^{224}Ra measurements in seawater and in suspended particles, the distribution coefficient of ^{224}Ra (K_d) at the river mouth fell in the range of 2500–11,000, much higher than in the mid-salinity region (Table 2). If ^{224}Ra is transported (i.e., by estuarine circulation) from the mid-salinity region characterized by high seawater ^{224}Ra activity and low K_d in the sediment to the river mouth characterized by low seawater ^{224}Ra activity and high K_d in the sediment, a fraction of ^{224}Ra in the overlying water may be absorbed by bottom sediment, resulting in a ^{224}Ra excess as observed in the upper 0–10 cm sediment at Y0.

Like other dissolved species in interstitial water, the benthic flux of ^{224}Ra must be regulated by the multiple processes that operate at the sediment–water interface. These processes include molecular diffusion, bioturbation, and irrigation. As shown in Fig. 7, at our study sites ^{224}Ra flux is positively correlated with the bioturbation coefficient ($F_{\mathrm{Ra}} = (-5.3 \pm 1.7) \times 10^4 D_B - (0.079 \pm 0.019)$; $R^2 = 0.708$; $P < 0.05$). The positive correlation indicates that bioturbation is an important process that regulates the benthic fluxes of ^{224}Ra in the Yangtze estuary. The intercept in this linear relation is -0.079 ± 0.019 dpm cm^{-2} d^{-1}, which represents the average ^{224}Ra flux resulted from other processes, namely molecular diffusion and irrigation. Of course, this intercept is meaningful only if K_d and ^{224}Ra activity in the overlying water are uniform for all the stations plotted.

The relative importance of molecular diffusion, bioturbation, and irrigation in regulating the benthic flux of ^{224}Ra can be assessed in a more quantitative manner by modeling the ^{224}Ra profiles using the general diagenetic equation (Berner, 1980):

$$\frac{\partial^{224}\mathrm{Ra}}{\partial t} = \frac{\partial\left(\frac{D_S}{K+1} \times \frac{\partial^{224}\mathrm{Ra}}{\partial z}\right)}{\partial z} + \frac{\partial\left(D_B \frac{\partial^{224}\mathrm{Ra}}{\partial z}\right)}{\partial z} - \frac{1}{\rho_s(1-\phi)} \times \frac{\partial F_g}{\partial z} - \omega\frac{\partial^{224}\mathrm{Ra}}{\partial z} - \lambda_{224}{}^{224}\mathrm{Ra} + \lambda_{224}{}^{228}\mathrm{Th} \quad (4)$$

where K is a dimensionless adsorption constant. It is linked to the distribution coefficient of ^{224}Ra by the relation $K = [\rho_s(1-ø)/ø] \times K_d$. D_S is the diffusivity of ^{224}Ra in the sediment, D_B represents the bioturbation coefficient, and F_g (dpm cm^{-2} d^{-1}) denotes the flux induced by irrigation. Note that ^{224}Ra in this expression takes a unit of dpm/g dry sediment. Eq. (4) implicitly assumes that the density of dry sediment (ρ_s) and porosity (ø) are constant with depth. In this expression, the first term on the right side represents the contribution of molecular diffusion of ^{224}Ra in interstitial water. The second term describes the contribution of bioturbation. The third term denotes the contribution of irrigation. The fourth term describes transport of ^{224}Ra by sedimentation. The fifth and sixth terms are decay and production rates of ^{224}Ra in the sediment. The molecular diffusion coefficient for radium in seawater (D) is a function of temperature. At 0–25 °C, it varies from 3.7×10^{-6} to 8.3×10^{-6} cm^2 s^{-1} (Boudreau, 1997). In marine sediments, this coefficient must be further corrected for tortuosity (θ) by the relation $D_S = D/\theta^2$. The tortuosity can be estimated from the porosity using the expression $\theta^2 = 1 - 2\ln(ø)$ (Boudreau, 1997). For the ^{224}Ra distribution in marine sediments, the advective burial of sediment is generally a small term compared to the decay or the production rate of ^{224}Ra (Hancock et al., 2000). Therefore, we neglected this small term in our model. Aside from Y0, Y1, and N0, ^{228}Th in the upper 0–10 cm sediment can be best approximated as an exponential function of depth. With these assumptions, we obtain an equation for the steady-state distribution of ^{224}Ra in the sediment:

$$\frac{\partial\left(\frac{D_S}{K+1} \times \frac{\partial^{224}\mathrm{Ra}}{\partial z}\right)}{\partial z} + \frac{\partial\left(D_B \frac{\partial^{224}\mathrm{Ra}}{\partial z}\right)}{\partial z} - \frac{1}{\rho_s(1-\phi)} \times \frac{\partial F_g}{\partial z} - \lambda_{224}{}^{224}\mathrm{Ra} + \lambda_{224}(Ge^{-\beta z} + S) = 0 \quad (5)$$

where G, β, and S can be identified by finding the best fits to the ^{228}Th profiles in the sediment. For Y0, Y1, and N0, we assume that ^{228}Th activity was constant in the upper 0–10 cm sediment. In this case, the steady-state distribution of ^{224}Ra in the sediment can be expressed as:

$$\frac{\partial\left(\frac{D_S}{K+1} \times \frac{\partial^{224}\mathrm{Ra}}{\partial z}\right)}{\partial z} + \frac{\partial\left(D_B \frac{\partial^{224}\mathrm{Ra}}{\partial z}\right)}{\partial z} - \frac{1}{\rho_s(1-\phi)} \times \frac{\partial F_g}{\partial z} - \lambda_{224}{}^{224}\mathrm{Ra} + \lambda_{224}S = 0 \quad (6)$$

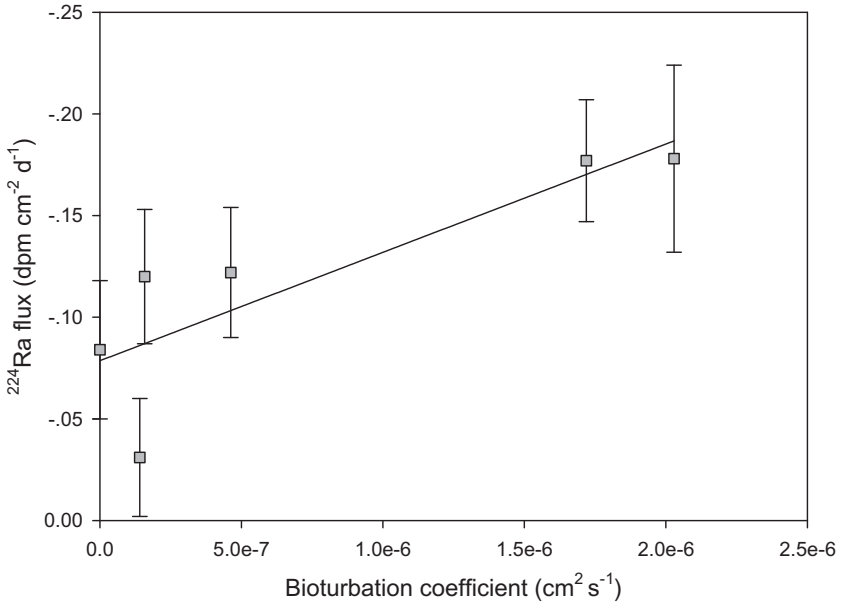

Fig. 7. Dependence of the measured flux of ^{224}Ra on the bioturbation coefficient in the sediment of the study region. Note that a negative value means flux from sediment to water.

In order to assess the relative importance of molecular diffusion plus bioturbation in the overall ^{224}Ra budget, we initially assume that irrigation is negligible. Under this circumstance, Eqs. (5) and (6) are simplified to:

$$\frac{\partial\left(\frac{D_S}{K+1}\times\frac{\partial^{224}\mathrm{Ra}}{\partial z}\right)}{\partial z}+\frac{\partial\left(D_B\frac{\partial^{224}\mathrm{Ra}}{\partial z}\right)}{\partial z}-\lambda_{224}{}^{224}\mathrm{Ra}+\lambda_{224}(Ge^{-\beta z}+S)=0 \quad (7)$$

and

$$\frac{\partial\left(\frac{D_S}{K+1}\times\frac{\partial^{224}\mathrm{Ra}}{\partial z}\right)}{\partial z}+\frac{\partial\left(D_B\frac{\partial^{224}\mathrm{Ra}}{\partial z}\right)}{\partial z}-\lambda_{224}{}^{224}\mathrm{Ra}+\lambda_{224}S=0 \quad (8)$$

To solve Eqs. (7) and (8), two boundary conditions are required. At the sediment–water interface, we assume that ^{224}Ra/^{228}Th ratio in the surface sediment is identical to the average ratio in suspended particles (γ), i.e., $^{224}\mathrm{Ra}=\gamma\times(G+S)$ or $^{224}\mathrm{Ra}=\gamma\times S$. At infinite depth, we have the boundary condition $^{224}\mathrm{Ra}=S$ as $z\to\infty$, i.e., assuming that ^{224}Ra is in secular equilibrium with ^{228}Th. The solutions to Eqs. (7) and (8) are:

$$^{224}\mathrm{Ra}=-\left[\frac{G[(1-\gamma)B+\gamma\beta^2]}{(B-\beta^2)}+(1-\gamma)S\right]e^{-\sqrt{B}z}+\frac{BG}{B-\beta^2}e^{-\beta z}+S \quad (9)$$

and

$$^{224}\mathrm{Ra}=S[1-(1-\gamma)e^{-\sqrt{B}z}] \quad (10)$$

where

$$B=\frac{(K+1)\lambda_{224}}{D_S+(K+1)D_B}$$

Eqs. (9) and (10) illustrate ^{224}Ra distribution in the near-surface sediment of the Yangtze estuary when molecular diffusion and bioturbation are the dominant processes that operate at the sediment–water interface. In this case, the flux of ^{224}Ra (F_{M+B}) across the sediment–water interface is given by

$$F_{M+B}=-\left(\frac{D_S}{K+1}+D_B\right)\rho_s(1-\phi)\times\left\{\left[\frac{G[(1-\gamma)B+\gamma\beta^2]}{(B-\beta^2)}+(1-\gamma)S\right]\sqrt{B}-\frac{BG\beta}{B-\beta^2}\right\} \quad (11)$$

and

$$F_{M+B}=-\left(\frac{D_S}{K+1}+D_B\right)\rho_s(1-\phi)(1-\gamma)S\sqrt{B} \quad (12)$$

If molecular diffusion is the only process that operates at the sediment–water interface, then the second term in Eqs. (7) and (8) is removed. In such a case, ^{224}Ra distribution and the diffusive flux of ^{224}Ra (F_M) are just a special case of the more general Eqs. (9)–(12) with $D_B=0$. In Eqs. (9)–(12), the value of K can be estimated from the distribution coefficient of ^{224}Ra, K_d. Previous studies have demonstrated that the value of K_d in bottom sediment generally falls in the range of 10–5000, with higher values in freshwater and lower values in seawater (Cochran and Krishnaswami, 1980; Krest and Harvey, 2003). In this study, we adopt a K_d value of 2500 to model the ^{224}Ra distribution at Y0. For the other sites, a K_d value of 11.7 (Hancock et al., 2000) is used to calculate the flux of ^{224}Ra. Note that in Eqs. (11) and (12), the term $1/(K+1)$ is not applied to D_B because a true random mixing process of sediment involves both solid particles and the

accompanying interstitial water. All the parameters used in the model calculation are listed in Table 4. Results of the flux calculation are also shown in Table 3. For Y0, Y1, and N0, F_{M+B} is not available because ^{234}Th excess was not detectable at these sites.

The flux of ^{224}Ra solely induced by molecular diffusion (F_M) varied between −0.025 and 0.001 dpm cm^{-2} d^{-1} (Table 3). The positive flux represents net absorption of ^{224}Ra from the overlying water by the bottom sediment. From Table 3, it is evident that at different locations the relative contribution of molecular diffusion was highly variable, ranging from <1% to 100% of the observed flux of ^{224}Ra. Nevertheless, for most study sites molecular diffusion can account for only ~10% of the measured flux of ^{224}Ra. Two exceptions are Y1 and Y18, where molecular diffusion was responsible for 100% and 58% of the benthic flux of ^{224}Ra. At Y0, molecular diffusion can explain only <1% of the ^{224}Ra excess in the upper 0–10 cm sediment. In comparison, when the process of bioturbation is incorporated, the flux of ^{224}Ra (F_{M+B}) increases by a factor of 2–3. It ranged from −0.009 to −0.057 dpm cm^{-2} d^{-1}, and on average, accounted for 30% of the observed flux of ^{224}Ra. Like molecular diffusion, the relative contribution of F_{M+B} to the total flux of ^{224}Ra at different locations was also quite variable. At Y4, it was responsible for 11% of the measured flux of ^{224}Ra. By contrast, at Y18 it explained up to 70% of the benthic flux of ^{224}Ra. In this regard, it must be noted that an important mechanism invoked by Eqs. (11) and (12) is that as sediment particles are brought to the sediment–water interface, a fraction of ^{224}Ra originally associated with solid particles can be released into the overlying water due to re-establishment of the absorption–desorption equilibrium of ^{224}Ra (Sun and Torgensen, 2001). Had this mechanism not been invoked, the term $1/(K+1)$ must be applied to D_B in the expression of flux calculation. Consequently, this would lead to an increase of only <0.0028 dpm cm^{-2} d^{-1} in the theoretical flux F_{M+B} compared to F_M. Clearly, this value is too small to explain the dependence of the measured flux of ^{224}Ra on the bioturbation coefficient as illustrated in Fig. 7.

Taking the uncertainty into consideration, only at Y1 and Y18 were molecular diffusion and bioturbation sufficient to account for the observed flux of ^{224}Ra. For most cases, these two mechanisms can explain only ~20–30% of the benthic flux of ^{224}Ra. Fig. 8 compares the measured profile of ^{224}Ra collected from Y3 with those calculated using Eq. (9). In general, the model-derived ^{224}Ra activities are higher than the actual measurements. We therefore conclude that other mechanisms, especially irrigation, must be invoked to explain the remaining 70% of the observed deviation of ^{224}Ra relative to ^{228}Th in the near-surface sediment of the Yangtze estuary. Irrigation can be treated as a process of pumping seawater into the seabed, and consequent advection upward of interstitial water (e.g., Smethie et al., 1981). Thus, for the irrigation term in Eq. (4) we specify that

$$\frac{\partial F_g}{\partial z} = \phi \frac{c_p - c_s}{\tau_z} \tag{13}$$

where c_p is the activity of ^{224}Ra per unit volume of pore water, c_s is the ^{224}Ra activity in the overlying water, and τ_z represents the residence time of pore water at depth z. Apart from the river mouth, ^{224}Ra activity in the overlying seawater is generally much lower than the pore water activity, i.e., $c_s \ll c_p$ (e.g., Hancock et al., 2000). As such, Eq. (13) can be re-written as

$$\frac{\partial F_g}{\partial z} = \frac{1}{\tau_z} \rho_s (1-\phi) \frac{^{224}\mathrm{Ra}}{K+1} \tag{14}$$

Direct measurement of the residence time of pore water, however, is exceedingly difficult. In this study, we used Eq. (14) to calculate the value of τ_z that is required to explain the observed flux of ^{224}Ra. In the calculation, we assumed that τ_z is constant in the zone of irrigation. In addition, both molecular diffusion and bioturbation were assumed to be active such that the flux of ^{224}Ra induced by irrigation (F_g) is equivalent to the difference between the measured flux and the flux caused by molecular diffusion plus bioturbation (F_{M+B}). Results of the calculation show that the average residence time of pore water in the

Table 4
Parameters used in the model calculation. D and D_S represent the molecular diffusion coefficient of radium in seawater and in the sediment, ø denotes the porosity in the sediment, K is a dimensionless adsorption constant, γ is the average ratio of ^{224}Ra/^{228}Th in suspended particles, G, β, and S are the constants identified by finding the best fits to the ^{228}Th profiles in the sediment. See text for the details.

Station	D (10^{-6} cm^2 s^{-1})	D_S (10^{-6} cm^2 s^{-1})	ø	K	γ	G (dpm/g)	β (cm^{-1})	S (dpm/g)
Y0	9.1	3.3	0.42	898	1.41[a]	–	–	0.64
Y1	8.5	4.2	0.60	20	0.60	–	–	0.75
Y3	8.0	4.4	0.67	15	0.60	1.24	0.16	0.00
Y4	7.3	2.8	0.44	39	0.60	0.26	1.89	0.37
Y8	7.5	3.0	0.47	35	0.60	0.24	0.79	0.37
Y10	7.9	3.6	0.55	25	0.60	0.50	0.78	0.42
Y17	7.9	3.8	0.58	22	0.60	0.39	0.49	0.63
Y18	7.5	4.2	0.68	15	0.60	0.63	0.20	0.29
N0	8.4	4.0	0.58	22	0.60	–	–	0.42

[a] At this location, we arbitrarily take an upper boundary condition that ^{224}Ra/^{228}Th ratio at the sediment–water interface is equivalent to the maximum ratio that was measured in the sediment core. Regardless of this boundary condition, a sensitivity test reveals that the diffusive flux (F_M) is a negligible term in the overall ^{224}Ra budget at this location.

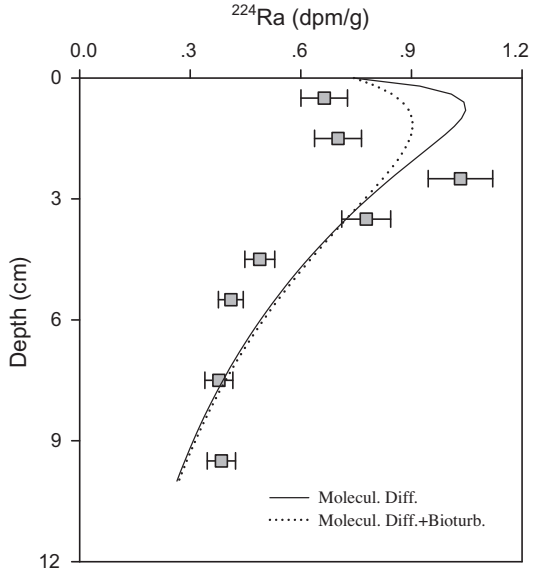

Fig. 8. Measured ^{224}Ra activities at Y3 compared to the theoretical profiles shaped solely by molecular diffusion (solid line), and by molecular diffusion plus bioturbation (dotted line).

upper 0–10 cm sediment of the Yangtze estuary varied between 1.5 and 34 d (Table 3). For most study sites, however, the residence time of pore water was in the vicinity of 2 d. In terms of a layer of 10 cm sediment, this residence time corresponds to an irrigation rate of 0.3–6.7 cm d^{-1}. Smethie et al. (1981) used ^{222}Rn budget in the sediment to estimate an irrigation rate of 0–4.4 cm d^{-1} on the Washington continental shelf. Colbert and Hammond (2008) reported a pore water residence time of 4 d for the top 28 cm of sediments in San Pedro Bay. This corresponds to an irrigation rate of 6.9 cm d^{-1}. Overall, our result from the Yangtze estuary compares well to those reported for the Washington continental shelf and San Pedro Bay.

We can use Eq. (13) to further explore site Y0 at the river mouth, where excess ^{224}Ra was measured in the upper sediments. This site is characterized by permeable sandy sediments. Because of the small scale turbulence in the upper layer of unconsolidated sediment caused by bottom swell and tidal currents (e.g., Rutgers van der Loeff, 1981), it is expected that irrigation at this site would be highly efficient. We have proposed that estuarine circulation transported some seawater containing elevated activities of ^{224}Ra from the mid-salinity region to the river mouth where ^{224}Ra was scavenged by the bottom sediment. We take a value of 1.0 dpm/l for c_s, which is typical of the ^{224}Ra activity in seawater from the mid-salinity region (Table 3) and assume that the pore water at the river mouth was depleted in ^{224}Ra (i.e., $c_p \approx 0$) and that the flux of ^{224}Ra induced by bioturbation is negligible (i.e., $F_g \approx F_{\mathrm{Ra}} - F_M$). The value of τ calculated from Eq. (13) is 0.010 ± 0.001 d. This corresponds to an irrigation rate of 990 ± 130 cm d^{-1}. It indicates that irrigation at Y0 was so efficient that the pore water in the upper 0–10 cm sediment at this site was flushed ~100 times each day, building an excess of ^{224}Ra in the sediments.

4.3. Transfer of other dissolved species: A ^{224}Ra/^{228}Th disequilibrium approach

The general diagenetic equation allowed us to model the ^{224}Ra profiles in the sediment. It has lent important insights into the mechanisms that control the exchange across the sediment–water interface in the Yangtze estuary. Using the derived estimates of D_S, D_B, and τ, it is possible to calculate the transfer rates of other dissolved species (like O_2, nutrient, and DIC). Nonetheless, it must be noted that several assumptions have to be invoked in order to derive an analytical solution to the general diagenetic equation. These assumptions include (a) that bioturbation is a true random mixing process such that it can be illustrated using an eddy-like diffusion coefficient D_B; (b) that other processes affecting the transfer of a dissolved species between the sediment and the overlying water, such as wave and current stirring, can be neglected; (c) the values of ρ_s, ø, K, D_S, and D_B in the sediment layer of interest are constant; and (d) that steady state is established. It is, however, not always possible to verify all of the assumptions.

In the present study, we propose a relatively simple and straightforward approach to quantify the transfer rate of a dissolved species across the sediment–water interface. This approach (hereafter referred to as the ^{224}Ra/^{228}Th disequilibrium approach) is built upon the observed ^{224}Ra/^{228}Th disequilibrium in the sediment and a concept of increased surface area for exchange by irrigation as developed by early investigators (e.g., Aller, 1980; Imboden, 1981). Fig. 9 is a schematic of this concept. In general, exchange of a dissolved species between the sediment and the overlying water is considered to take place not only at the conventional sediment–water interface, but also within the animal burrows and tubes in the sediment. In other words, the boundary layer for exchange is a highly invaginated interface. In addition, near the sediment–water interface and the wall of the burrows, there is a viscous sublayer where the concentration gradient of a dissolved species is established. This viscous sublayer results from the fact that the eddy diffusivity of a turbulent flow decreases and approaches to zero when the sediment surface (or the wall of burrows) is approached. As a consequence, molecular processes become quantitatively more important than turbulence in bringing about the transfer of dissolved constituents, i.e., molecular diffusion is the predominant transport mechanism of a dissolved species between the sediment and the overlying water (Jørgensen, 2006). If one further assumes that the burrows are constantly flushed so that the concentration gradient inside the burrows is the same as in the surface sediment, then the steady-state flux of a dissolved species can be written as

$$F = -\xi \phi D_S \frac{\partial c}{\partial z} \tag{15}$$

where ξ is an area factor, which can be regarded as the effective area available for the transfer of a dissolved species per unit area of wet sediment; $\frac{\partial c}{\partial z}$ is the concentration gradient of the species of interest at the interface. Eq. (15) is the general expression of the concept of increased surface area for exchange by irrigation. This general expression was first

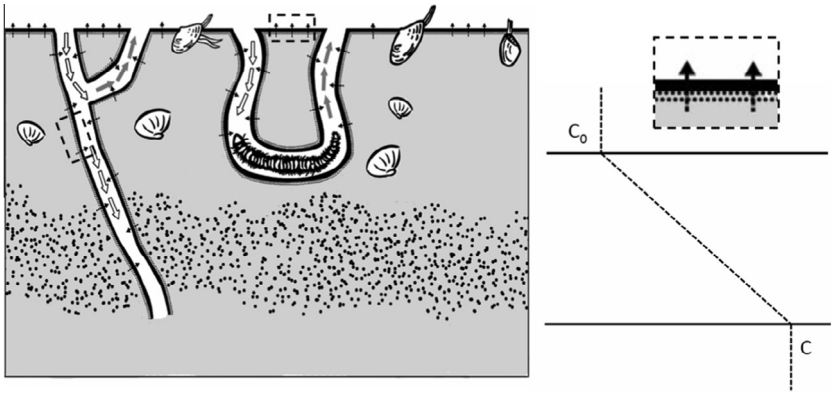

Fig. 9. A schematic of the general concept of increased surface area for exchange by irrigation. The viscous sublayer adjacent to the sediment–water interface is indicated by a framed box (left graph) and is blown up in the right graph.

proposed as a non-local transport process by Imboden (1981). Christensen et al. (1984) showed that the non-local transport process can be interpreted as reflecting increased surface area of sediments. Hammond et al. (1985) pursued this general concept and used ^{222}Rn as a tracer to assess nutrient exchange in estuarine sediments. By virtue of ^{222}Rn, Colbert and Hammond (2008) applied a related model to coastal sediments to calculate pore water residence times. These investigators showed that pore water ^{224}Ra and ^{223}Ra had residence times similar to ^{222}Rn. Although considerable success has been made, one limitation of Eq. (15), however, lies in its inherent assumption that irrigation channels maintain a concentration that is equal to the concentration in the overlying water. If the irrigation channels have a significant residence time, the burrow water will approach pore water concentrations at depth. Under this circumstance, the flux of a dissolved species will be overestimated by Eq. (15) (Hammond et al., 1985).

Based on the flux of ^{224}Ra (F_{Ra}) derived from ^{224}Ra/^{228}Th disequilibrium in the sediment, ξ can be calculated from Eq. (15). Consequently, the benthic flux of a dissolved species i (F_i) is expressed by

$$F_i = F_{\mathrm{Ra}}\left(\frac{D_S^i}{D_S^{\mathrm{Ra}}}\right)\left(\frac{\frac{\partial c^i}{\partial z}}{\frac{\partial c^{\mathrm{Ra}}}{\partial z}}\right) \tag{16}$$

where superscript Ra and i denote ^{224}Ra and the dissolved species i, respectively. In practice, when high-resolution profiles of pore water ^{224}Ra and i are not available, the concentration gradients $\frac{\partial c^{\mathrm{Ra}}}{\partial z}$ and $\frac{\partial c^i}{\partial z}$ can be determined by measuring the ^{224}Ra activity and the concentration of i in the overlying water and at the layer of 0–1 cm sediment. The uncertainty with F_i depends mainly on the error associated with the measured flux of ^{224}Ra and on how accurately we can characterize the concentration gradients of ^{224}Ra and i at the interface. For the ratio of molecular diffusion coefficient D_S^i to D_S^{Ra}, however, it is not different from the ratio in seawater. Moreover, this ratio is constant over the temperature range of 0–25 °C that is generally encountered in the sediment (Boudreau, 1997). As such, calculation of the individual molecular diffusion coefficient in the sediment is unnecessary, and the error caused by the correction for tortuosity and temperature is thus eliminated. Compared to the theoretical approach based on the general diagenetic equation, the ^{224}Ra/^{228}Th disequilibrium approach eliminates the need to resort to highly idealized parameters, such as K, D_B, and τ. Instead, the transfer of a dissolved species is simplified as molecular diffusive processes across a highly invaginated sediment–water interface. Overall, the ^{224}Ra/^{228}Th disequilibrium approach is fairly easy to apply.

We now use this approach to quantify the benthic consumption rate of dissolved O_2 (DO) in the Yangtze estuary. Depth profiles of DO in the sediment were determined at Y1, Y3, Y10, Y17, and Y18 using a Hg–Au microelectrode. As shown in Fig. 10, DO dropped from ~150–210 μM to zero over the top few millimeters of the sediment. We estimated the concentration gradient of DO by finding the best fit of DO vs. depth to a straight line. The derived gradient of DO in the sediment varied from −0.25 to −0.75 μmol cm^{-4}. Using the K_d value adopted above, the concentration gradient of pore water ^{224}Ra can be inferred from the measurements of total ^{224}Ra activity in 0–1 cm sediment. The ratio of molecular diffusion coefficient $D_S^{O_2}$ to D_S^{Ra} in the sediment is 2.6 (Boudreau, 1997). On the basis of the measured flux of ^{224}Ra, we derive an estimate of 1.2 ± 3.4 to 25.6 ± 4.4 mmol O_2 m^{-2} d^{-1} for the benthic consumption rate of dissolved O_2 in the Yangtze estuary (Table 3). In this study, water column O_2 uptake experiments were also conducted. The results showed that at the study sites, the oxygen utilization rates in the bottom of the water column ranged from 20.6 to 110.3 mmol O_2 m^{-2} d^{-1} (Table 3). The benthic consumption rate of dissolved O_2 is equivalent to 6–61% of the utilization rate of O_2 in the bottom water. Thus, benthic consumption represents an important loss term of dissolved O_2 in the Yangtze estuary and must be considered as one of the mechanisms that lead to hypoxia in this area (Li et al., 2002; Wang, 2009).

5. SUMMARY

Transfer across the sediment–water interface is critical to understanding the biogeochemistry of many elements in the coastal seas. In this study, ^{224}Ra/^{228}Th disequilibrium

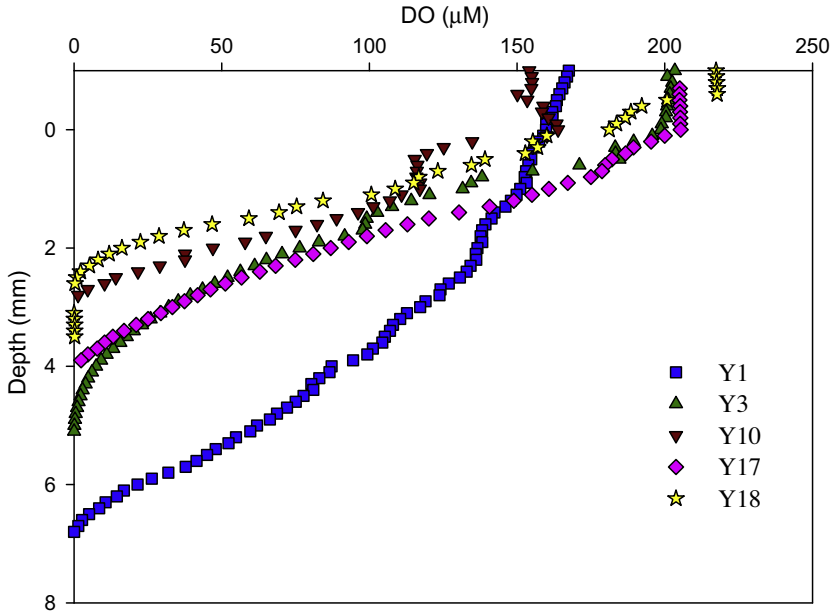

Fig. 10. Depth profiles of dissolved O_2 in the sediment at different study sites.

was first used to investigate the processes that regulate the exchange between the sediment and the overlying water in the Yangtze estuary. By modeling the ^{224}Ra profiles in the sediment using the general diagenetic equation, we demonstrated that in most cases molecular diffusion and bioturbation together can account for only ~20–30% of the measured flux of ^{224}Ra. We concluded that other mechanisms, especially irrigation, must be invoked to explain the remnant 70% of the observed deviation of ^{224}Ra relative to ^{228}Th in the sediment. On the basis of the ^{224}Ra/^{228}Th disequilibrium in the sediment and a concept of increased surface area for exchange by irrigation as developed by early investigators, we proposed a new approach – the ^{224}Ra/^{228}Th disequilibrium approach to quantify the transfer rate of other dissolved species across the sediment–water interface. We have utilized this new approach to determine the benthic consumption rate of dissolved O_2. The result reveals that benthic consumption is an important loss term of dissolved O_2 in the Yangtze estuary and must be considered as one of the mechanisms that lead to hypoxia in this area.

The principal restrictions of the ^{224}Ra/^{228}Th disequilibrium approach are our ability to measure the flux of ^{224}Ra, how accurately we can characterize the concentration gradients of pore water ^{224}Ra and the dissolved species of interest at the interface, and how uniform the concentration gradient is at each site. In this study, the concentration gradients of pore water ^{224}Ra were inferred from the measurements of total ^{224}Ra activity in the sediment. A sensitivity test reveals that the calculated fluxes of oxygen are rather sensitive to the value of K_d that is selected. For changes of 2× in the K_d value of ^{224}Ra, the calculated oxygen fluxes would change by approximately the same factor. Direct measurement of high-resolution profiles of pore water ^{224}Ra should therefore be considered to be the top priority in future studies. Inter-comparison between the ^{224}Ra/^{228}Th disequilibrium approach and the traditional approaches, such as a benthic chamber approach, should also be encouraged.

ACKNOWLEDGMENTS

This work was supported by the National Basic Research Program ("973" Program) of China through Grant No. 2009CB421203 and by the Natural Science Foundation of China (NSFC) through grants 41076041 and 41276062. Support to this work also came from the funds for creative research groups of the National Natural Science Foundation of China (Grant No. 41121091). The authors thank S. J. Kao and L.T.J. Hsu for providing the dissolved oxygen data in the sediment. Thanks are also due to Dr. M.M. Rutgers van der Loeff and two anonymous reviewers for their constructive comments. PC would like to dedicate this paper to BB for the inspiration of research.

REFERENCES

Aller R. C. (1980) Diagenetic processes near the sediment–water interface of Long Island Sound, I. Decomposition and nutrient element geochemistry (S, N, P). In *Estuarine Physics and Chemistry: Studies in Long Island Sound*, vol. 22 (ed. B. Saltzman). Academic Press, New York.

Aller R. C. and Cochran J. K. (1976) ^{234}Th/^{238}U disequilibrium in near-shore sediment: particle reworking and diagenetic time scales. *Earth Planet. Sci. Lett.* **29**, 37–50.

Anderson R. F. and Fleer A. P. (1982) Determination of natural actinides and plutonium in marine particulate material. *Anal. Chem.* **54**, 1142–1147.

Berelson W. M., Hammond D. E. and Johnson K. S. (1987) Benthic fluxes and the cycling of biogenic silica and carbon in two Southern California borderland basin. *Geochim. Cosmochim. Acta* **51**, 1345–1363.

Berner R. A. (1980) *Early Diagenesis – A Theoretical Approach*. Princeton University Press, Princeton, New Jersey.

Boudreau B. P. (1997) *Diagenetic Models and Their Implementation: Modelling Transport and Reactions in Aquatic Sediments*. Springer-Verlag, Berlin, Heidelberg, NY, 414pp.

Broecker W. S., Kaufman A. and Trier R. M. (1973) The residence time of thorium in surface sea water and its implications regarding the rate of reactive pollutants. *Earth Planet. Sci. Lett.* **39**, 37–50.

Buesseler K. O., Benitez-Nelson C., Rutgers van der Loeff M., Andrews J., Ball L., Crossin G. and Charette M. (2001) An intercomparison of small- and large-volume techniques for thorium-234 in seawater. *Mar. Chem.* **74**, 15–28.

Cai P., Dai M., Lv D. and Chen W. (2006) An improvement in the small-volume technique for determining thorium-234 in seawater. *Mar. Chem.* **100**, 282–288.

Cai P., Shi X., Moore W. S. and Dai M. (2012) Measurement of ^{224}Ra:^{228}Th disequilibrium in coastal sediments using a delayed coincidence counter. *Mar. Chem.* **138–139**, 1–6.

Changjiang Water Conservancy (2010) *Changjiang Sediment Bulletin in 2009*. Changjiang Press, Wuhan, 35pp (in Chinese).

Chen Z., Li J., Shen H. and Wang Z. (2001) Yangtze River of China: historical analysis of discharge variability and sediment flux. *Geomorphology* **41**, 77–91.

Christensen J. P., Devol A. H. and Smethie W. M. (1984) Biological enhancement of solute exchange between sediments and bottom water on the Washington continental shelf. *Cont. Shelf Res.* **3**, 9–23.

Cochran J. K. and Aller R. C. (1979) Particle reworking in sediments from the New York Bight apex: evidence from ^{234}Th/^{238}U disequilibrium. *Estuarine Coastal Mar. Sci.* **9**, 739–747.

Cochran J. K. and Krishnaswami S. (1980) Radium, thorium, uranium, and ^{210}Pb in deep-sea sediments and sediment pore waters from the north equatorial Pacific. *Am. J. Sci.* **280**, 849–889.

Colbert S. L. and Hammond D. E. (2008) Shoreline and seafloor fluxes of water and short-lived Ra to surface water of San Pedro Bay, CA. *Mar. Chem.* **108**, 1–17.

DeMaster D. J., Nittrouer C. A., Cutshall N. H., Larsen I. L. and Dion E. P. (1980) Short-lived radionuclide profiles and inventories from Amazon continental shelf sediments. *Trans. Am. Geophys. Union* **61**, 1004.

DeMaster D. J., McKee B. A., Nittrouer C. A., Qian J. and Cheng G. (1985) Rates of sediment accumulation and particle reworking based on radiochemical measurements from continental shelf deposits in the East China Sea. *Cont. Shelf Res.* **4**, 143–158.

Emerson S., Jahnke R. and Heggie D. (1984) Sediment–water exchange in shallow water estuarine sediments. *J. Mar. Res.* **42**, 709–730.

Gu H., Moore W. S., Zhang L., Du J. and Zhang J. (2012) Using radium isotopes to estimate the residence time and the contribution of submarine groundwater discharge (SGD) in the Changjiang effluent plume, East China Sea. *Cont. Shelf Res.* **35**, 95–107.

Hammond D. E., Fuller C., Harmon D., Hartman B., Korosec M., Miller L. G., Rea R., Warren S., Berelson W. and Hager S. (1985) Benthic fluxes in San Francisco Bay. *Hydrobiologia* **129**, 69–90.

Hancock G. J., Webster I. T., Ford P. W. and Moore W. S. (2000) Using Ra isotopes to examine transport processes controlling benthic fluxes into a shallow estuarine lagoon. *Geochim. Cosmochim. Acta* **64**, 3685–3699.

Imboden D. M. (1981) Tracers and mixing in the aquatic environment: a critical discussion of diffusion models and an introduction into concepts of non-Fickian transport. Ph.D. thesis, Swiss Federal Institute of Technology, 137pp.

Jahnke R. A., Nelson J. R., Marinelli R. L. and Eckman J. E. (2000) Benthic flux of biogenic elements on the Southwestern US continental shelf: influence of pore water advective transport and benthic microalgae. *Cont. Shelf Res.* **20**, 109–127.

Jørgensen B. B. (2006) Bacteria and marine biogeochemistry. In *Marine Geochemistry* (eds. H. D. Schulz and M. Zabel), second ed. Springer-Verlag, Berlin, Heidelberg, pp. 169–206.

Krest J. M. and Harvey J. W. (2003) Using natural distributions of short-lived radium isotopes to quantify groundwater discharge and recharge. *Limnol. Oceanogr.* **48**, 290–298.

Krest J. M., Moore W. S. and Rama (1999) Radium-226 and radium-228 in the mixing zone of the Mississippi and Atchafalaya Rivers: indicators of groundwater input. *Mar. Chem.* **64**, 129–152.

Lee H.-J. and Chao S.-Y. (2003) A climatological description of circulation in and around the East China Sea. *Deep Sea Res. II* **50**, 1065–1084.

Lettmann K. A., Riedinger N., Ramlau R., Knab N., Bottcher M. E., Khalili A., Wolff J.-O. and Jørgensen B. B. (2012) Estimation of biogeochemical rates from concentration profiles: a novel inverse method. *Estuarine Coastal Shelf Sci.* **100**, 26–37.

Li D., Zhang J., Huang D., Wu Y. and Liang J. (2002) Oxygen depletion off the Changjiang (Yangtze River) estuary. *Sci. China Ser. D* **45**, 1137–1146.

Liu Z. (1988) The benthic fauna in the Yangtze River estuary. In *Zhong Guo Hai Wan Zhi*, vol. 14 (ed. Z. Chen). Ocean Press, Beijing.

Liu M. (2007) The exchange of nutrients across the sediment–water interface in the salt marsh of the Yangtze River estuary. In *The Biogeochemical Processes Regulating the Exchange of Nutrients Across the Sediment–Water Interface in the Yangtze River Estuary* (eds. M. Liu, S. Xu and L. Hou). Science Press, Beijing, pp. 111–162.

Liu J. P., Li A. C., Xu K. H., Velozzi D. M., Yang Z. S., Milliman J. D. and DeMaster D. J. (2006) Sedimentary features of the Yangtze River-derived along-shelf clinoform deposit in the East China Sea. *Cont. Shelf Res.* **26**, 2141–2156.

Liu Q., Dai M., Chen W., Huh C. A., Wang G., Li Q. and Charette M. A. (2012) How significant is submarine groundwater discharge and its associated dissolved inorganic carbon in a river-dominated shelf system? *Biogeosciences* **9**, 1777–1795.

Milliman J. D., Shen H. T., Yang Z. S. and Meade R. H. (1985) Transport and deposition of river sediment in the Changjiang estuary and adjacent continental shelf. *Cont. Shelf Res.* **4**, 37–45.

Moore W. S. (2008) Fifteen years experience in measuring ^{224}Ra and ^{223}Ra by delayed-coincidence counting. *Mar. Chem.* **109**, 188–197.

Moore W. S. and Arnold R. (1996) Measurement of ^{223}Ra and ^{224}Ra in coastal waters using a delayed coincidence counter. *J. Geophys. Res.* **101**, 1321–1329.

Moore W. S. and Krest J. (2004) Distribution of ^{223}Ra and ^{224}Ra in the plumes of the Mississippi and Atchafalaya Rivers and the Gulf of Mexico. *Mar. Chem.* **86**, 105–119.

Moore W. S., Astwood H. and Lindstrom C. (1995) Radium isotopes in coastal waters on the Amazon shelf. *Geochim. Cosmochim. Acta* **59**, 4285–4298.

Moore W. S., DeMaster D. J., Smoak J. M., Mckee B. A. and Swarzenski P. W. (1996) Radionuclide tracers of sediment–water interactions on the Amazon shelf. *Cont. Shelf Res.* **16**, 645–665.

Rutgers van der Loeff M. M. (1981) Wave effects on sediment water exchange in a submerged sand bed. *Netherlands J. Sea Res.* **15**, 100–112.

Rutgers van der Loeff M. M., Cai P., Stimac I., Bracher A., Middag R., Klunder M. B. and van Heuven S. M. A. C. (2011)

Th-234 in surface waters: distribution of particle export flux across the Antarctic Circumpolar Current and in the Weddell Sea during the GEOTRACES expedition ZERO and DRAKE. *Deep Sea Res. II* **58**, 2749–2766.

Santschi P. H., Murray J. W., Baskaran M., Benitez-Nelson C. R., Guo L., Hung C.-C., Lamborg C., Moran S. B., Passow U. and Roy-Barman M. (2006) Thorium speciation in seawater. *Mar. Chem.* **100**, 250–268.

Sayles F. L. (1979) The composition and diagenesis of interstitial solutions—I. Fluxes across the seawater–sediment interface in the Atlantic Ocean. *Geochim. Cosmochim. Acta* **43**, 526–546.

Smethie W. M., Nittrouer C. A. and Self R. F. L. (1981) The use of ^{222}Rn as a tracer of sediment irrigation and mixing of the Washington continental shelf. *Mar. Geol.* **42**, 173–200.

Smoak J. M., DeMaster D. J., Kuehl S. A., Pope R. H. and Mckee B. A. (1996) The behavior of particle-reactive tracers in a high turbidity environment: ^{234}Th and ^{210}Pb on the Amazon continental shelf. *Geochim. Cosmochim. Acta* **60**, 2123–2137.

Sun Y. and Torgensen T. (2001) Adsorption–desorption reactions and bioturbation transport of ^{224}Ra in marine sediments: a one-dimensional model with applications. *Mar. Chem.* **74**, 227–243.

Swarzenski P. W., Porcelli D., Andersson P. S. and Smoak J. M. (2003) The behavior of U- and Th-series nuclides in the estuarine environment. *Rev. Mineral. Geochem.* **52**, 577–606.

Wang B. D. (2009) Hydromorphological mechanisms leading to hypoxia off the Changjiang estuary. *Mar. Environ. Res.* **67**, 53–58.

Yang S. L., Zhang J. and Xu X. J. (2007) Influence of the Three Gorges Dam on downstream delivery of sediment and its environmental implications, Yangtze River. *Geophys. Res. Lett.* **34**, L10401.

Associate editor: S. Krishnaswami